Journal of Alloys and Compounds 509 (2011) 9977–9985

Contents lists available at ScienceDirect

Journal of Alloys and Compounds

journal homepage: www.elsevier.com/locate/jallcom

Study of manganese ferrite powders prepared by a soft mechanochemical route

Z.Ž. Lazarević[a,*], Č. Jovalekić[b], A. Recnik[c], V.N. Ivanovski[d], M. Mitrić[d], M.J. Romčević[a], N. Paunović[a], B.Đ. Cekić[d], N.Ž. Romčević[a]

[a] Institute of Physics, University of Belgrade, P.O. Box 68, Pregrevica 118, Zemun, Belgrade, Serbia
[b] The Institute for Multidisciplinary Research, University of Belgrade, Kneza Višeslava 1, Belgrade, Serbia
[c] Department for Nanostructured Materials, Jožef Stefan Institute, Ljubljana, Slovenia
[d] Institute of Nuclear Sciences Vinča, University of Belgrade, P.O. Box 522, 11001 Belgrade, Serbia

ARTICLE INFO

Article history:
Received 11 January 2011
Received in revised form 1 August 2011
Accepted 3 August 2011
Available online 16 August 2011

Keywords:
Mehanochemical processing
TEM
Magnetic measurements
Mössbauer spectroscopy

ABSTRACT

Manganese ferrite, $MnFe_2O_4$ have been prepared by a soft mechanochemical route from mixture of (a) $Mn(OH)_2$ and α-Fe_2O_3 and (b) $Mn(OH)_2$ and $Fe(OH)_3$ powders in a planetary ball mill. The mixture was activated for varying duration. Soft mechanochemical reaction leading to formation of the $MnFe_2O_4$ spinel phase was followed by X-ray diffraction, Raman spectroscopy, scanning and transmission microscopy and magnetization measurements. The spinel phase formation was first observed after 12 h of milling and its formation was completed after 25 h in both cases. The synthesized $MnFe_2O_4$ ferrite has a nanocrystalline structure with a crystallite size of about 40 and 50 nm respectively for cases (a) and (b). There are five Raman active modes. Measurements after 25 h of milling show magnetization values of 70.4 emu/g and 71.1 emu/g respectively for cases (a) and (b). In order to understand better the whole process of phase formation, Mössbauer measurements were done.

1. Introduction

Ferrites are one of the best magnetic ceramics used in many technological applications such as high frequency magnetic materials, recording media, ferrofluid technology, sensor technology, and microwave applications [1–5]. The magnetic and electrical properties of spinel ferrites are of academic and technical interest and are dependent on the chemical composition, cation distribution, grain size and the method of preparation [6].

The soft magnetic ferrites are materials which crystallize in cubic spinel structure, spatial or point symmetry group *Fd3m*. The chemical formula of the spinel ferrite can be written as MFe_2O_4, where *M* is a metal or a group of metallic elements with 2 total valence [4]. The M^{2+} and Fe^{3+} cations can be distributed into two crystal sites of spinel structure: tetrahedral sites and octahedral sites. Typically two extreme type of spinel structure can be found: normal spinel and inverse spinel, but in practice mixed spinel structure are also observed. Basic structure of a spinel ferrite is MFe_2O_4, where *M* is divalent metal ion (*M* = Mg, Ni, Zn, Mn. . .). In a unit cell of the spinel lattice there are eight tetrahedral and sixteen octahedral sites occupied by *M* and Fe^{3+} cations, while the oxygen anions are arranged in a cubic close packed structure. Site occupancy may range from the normal spinel structure, in which *M* cations occupy the tetrahedral sites and Fe^{3+} the octahedral ones, to the inverse spinel, in which half the Fe^{3+} cations occupy the tetrahedral sites, and both *M* and Fe^{3+} cations occupy the octahedral sites. In general, site occupancy in $MnFe_2O_4$ may be expressed by rewriting its generic formula as $(Mn_{1-x}Fe_x)[Mn_xFe_{1-x}]O_4$, where parentheses and square brackets denote tetrahedral and octahedral sites, respectively, *x* represents the so called degree of inversion, defined as the fraction of tetrahedral sites occupied by Fe^{3+} cations [5–7].

Many studies have been focused on the synthesis of metal oxide nanoparticles such as $MnFe_2O_4$. Ferrites are often prepared by high-temperature solid-state reactions [8]. In the last decades, nanoferrites exhibiting novel properties have been prepared by a variety of methods such as co-precipitation [9], sol–gel [10], hydrothermal reactions [11,12], combustion synthesis [13,14] and high-energy milling [15–20]. The latter method can deliver nanocrystalline ferrites (and complex oxides in general) in a one step process either by particle size reduction of bulk material to the nanometer scale without changes in its chemical composition or by inducing a heterogeneous solid-state chemical reaction between the ferrite precursors, i.e., by the mechanically induced formation reaction (mechanosynthesis) [7].

It is well known that properties of materials are influenced primarily by their chemical compositions, but also by their microstructure. Therefore the nanostructure materials exhibit unusual physical and chemical properties, significantly different from those of conventional bulk materials, due to their extremely small grain size or large specific surface area. Mechanochemical

* Corresponding author. Tel.: +381 11 37 13 035; fax: +381 11 31 60 531.
E-mail address: lzorica@yahoo.com (Z.Ž. Lazarević).

0925-8388/$ – see front matter © 2011 Elsevier B.V. All rights reserved.
doi:10.1016/j.jallcom.2011.08.004

treatment is a non-equilibrium solid-state process in which the final product retains a very fine, typically nanocrystalline or amorphous structure [21].

Mechanochemical treatment has been recognized as a powerful technique for synthesis of a wide range of materials. Thus, complex, multicomponent metallic and ceramic materials, which may otherwise be difficult to prepare by conventional high temperature treatment, have been successfully prepared by milling. Novel approach to mechanochemical synthesis, based on reactions of solid acids, based hydrated compounds, crystal hydrates, basic and acidic salts, has been called soft mechanochemical synthesis. The dissolved substances in the solid state substantially change their nature. It can influence on the comparison and properties of the final product. Peculiarities of soft mechanochemical reactions consist in the high reactivity of surface functional groups, notably, OH groups.

In this paper, we present the formation of spinel ferrite phase through soft mechanochemical treatment [22], starting from different mixtures of materials. The cases were:

(a) milling of mixture of $Mn(OH)_2 + \alpha\text{-}Fe_2O_3$ during 3–25 h;
(b) milling of mixture of $Mn(OH)_2 + Fe(OH)_3$ during 3–25 h.

During mechanochemical treatment, synthesis occurred in two stages. The first of the two stages was marked by the evolution of water vapor. The second stage was the formation of ferrite materials by solid state reactions. Preparation from ultra-fine powder is more advantageous since the composition can be more easily controlled, and properties are improved as a result of the reduced grain size [22].

Some articles indicate that the cation distribution in mechanosynthesized nanoscale ferrites is different from that in materials prepared by the conventional ceramic method [23,24]. According to these studies, the magnetization of ultrafine particles is extraordinary large compared with that of bulk materials due to the fact that a fairly large number of Fe^{3+} ions occupy (*A*) sites and form magnetic clusters with the nearest Fe^{3+} [*B*]-site neighbors through coupling by (*A*)–[*B*] interactions. The dependence of the integrated intensity ratio on the milling time revealed that the milling process induces cation redistribution between (*A*) and [*B*] sites. There have been numerous previous Mössbauer studies of $MnFe_2O_4$ [16,25]. In order to gain more information regarding the atomic disorder in mechanically activated $MnFe_2O_4$, we have undertaken a Mössbauer study of the mechanically induced structural evolution of this solid.

Raman spectroscopy in addition to the X-ray diffraction, scanning electron microscopy, transmission electron microscopy and magnetic and Mössbauer spectroscopy measurements were used to study the samples mechanochemically treated for different milling times.

2. Experimental procedures

For mixtures of crystalline powders, denoted by (a) and (b), the starting materials were: (a) manganese(II)-hydroxide (Merck 95% purity) and $\alpha\text{-}Fe_2O_3$ (Merck 99% purity); (b) manganese(II)-hydroxide (Merck 95% purity) and $Fe(OH)_3$ in equimolar ratio. The $Fe(OH)_3$ powder was made by adding equimolar amounts of NaOH solution (25% mass), made from 99% purity NaOH (Merck) to the $FeCl_3$ solution (25% mass), made from 99% purity $FeCl_3 \cdot 6H_2O$ (Merck). Dark brown precipitate was filtrated, washed with large amounts of water and dried in a vacuum desiccator. Before milling, the $Fe(OH)_3 \cdot nH_2O$ powder was heated at 105 °C for 24 h. Material prepared by this way had 99.5% $Fe(OH)_3$. It defined by potentiometric redox titration. X-ray analysis confirmed that the sample was amorphous, with a small amount of crystalline phase.

Mechanochemical synthesis was performed in air atmosphere in planetary ball mill (Fritsch Pulverisette 5). A hardened-steel vial of 500 cm^3 volume, filled with 40 hardened steel balls with a diameter of 13.4 mm, was used as the milling medium. The mass of the powder was 20 g and the balls-to-powder mass ratio was 20:1. The milling was done in air atmosphere without any additives. The angular velocity of the supporting disc and vial was about 32 and 40 rad s^{-1}, respectively. The intensity of milling corresponded to an acceleration of about 10 times the gravitation acceleration. All samples, with different starting compositions and milling times, were prepared and milled separately. At the expiration of the selected milling times (3, 12 and 25 h) the mill was stopped and a small amount of powder was removed from the vial for examination.

Characterization of the obtained samples was carried out by:

- X-ray diffraction analysis of powders treated for various periods of milling times by a Philips PW 1050 diffractometer equipped with a PW 1730 generator (40 kV × 20 mA) using Ni filtered CuKα radiation at the room temperature. Measurements were done in 2θ range of 10–80° with scanning step width of 0.05° and 10 s scanning time per step. After XRD measurements, the powder was placed back in a vial to obtain the same grinding conditions (balls to powder weight ratio).
- Room temperature Raman spectra in spectral range from 100 to 1200 cm^{-1}, in back scattering geometry, obtained by Jobin-Ivon T64000 monochromator using 514 nm of a frequency argon ion laser liner. The average power density on the sample was about 20 mW mm^{-2}.
- The morphology of powders and the size of soft mechano-synthesized ferrite crystallites were examined by scanning electron microscopy (SEM, Model TESCAN Vega TS130MM) and transmission electron microscopy (200 kV TEM, Model JEM-2100 UHR, Jeol Inc., Tokyo, Japan). Electron energy dispersive X-ray spectrometer (EDS) was used to examine the chemical composition of the product.
- The mechanochemical reaction was also followed by magnetization measurement at room temperature using VSM 200-Cryogenic magnetometer for the samples mechanochemically treated at different milling times.
- The Mössbauer spectra of powdered samples were measured at room temperature (RT) using a source of ^{57}Co in Rh (1.85 GBq). The experiments were performed in standard transmission geometry with constant acceleration calibrated by the laser spectrum. The data were analyzed by The WinNormos Site program [26]. Sample thickness correction was carried out by transmission integral.

3. Results and discussion

Soft mechanochemical synthesis and mechanical milling of (a) $Mn(OH)_2 + Fe_2O_3 \rightarrow MnFe_2O_4 + H_2O$ and (2) $Mn(OH)_2 + 2Fe(OH)_3 \rightarrow MnFe_2O_4 + 4H_2O$ was also carried out under air atmosphere. Fig. 1a shows the X-ray diffraction patterns of powders (a) mechanochemically milled for different milling times (3, 12 and 25 h). The XRD pattern of the starting powder is characterized by sharp diffraction peaks corresponding to crystalline $Mn(OH)_2$ (JCPDS card 73-1133) and $\alpha\text{-}Fe_2O_3$ (JCPDS card 89-8103) [27]. With increasing milling time, the diffraction peaks corresponding to the simple oxide and hydroxide gradually disappear. All the characteristic peaks of $Mn(OH)_2$ and $\alpha\text{-}Fe_2O_3$ are well pronounced in the spectrum (Fig. 1a). During mechanochemical treatment (3 h) only sharp peaks from the well-crystallized $Mn(OH)_2$ and $\alpha\text{-}Fe_2O_3$ are present in the XRD pattern. It can be noticed that the major peaks for the hematite phase at $2\theta = 35.6°$ and 33.15° were continuously reduced by increasing the milling time (Fig. 1a). It can be observed slightly wider peaks $\alpha\text{-}Fe_2O_3$ lower intensity and almost disappeared peaks $Mn(OH)_2$. It is important to note that during the milling of powder mixtures between 3 and 12 h occurs and a new phase FeO(OH) (JCPDS card 89-6096) and MnO (JCPDS card 75-1090). The main reason for this phenomenon is because $Mn(OH)_2$ quickly decomposes through $Mn(OH)_2 \rightarrow MnO + H_2O$, so that after 3 h of milling (Fig. 1a) there are no peaks corresponding to the starting compound $Mn(OH)_2$. It is known that the milling process leads to overheating of the vessel, and at temperatures higher than 100 °C leading to the evolution of water vapor. Opening the container comes to partial evaporation of water. It might be noted that the hydroxides transform into oxides. At the same time, it can be observed the peaks characteristic of the hydroxide and oxide (Fig. 1a). This may be a consequence of opening of the milling vessel. Also, overpressure of gasses in the vessel reduced the efficiency of milling, especially in the case of water vapor where the effect of soft milling also emerged and additionally reduced the efficiency of obtaining of the new phase. The reason is almost the same for the samples obtained from the mixture of powders for 12 h of milling time. This means that there is no complete decomposition of hydroxide.

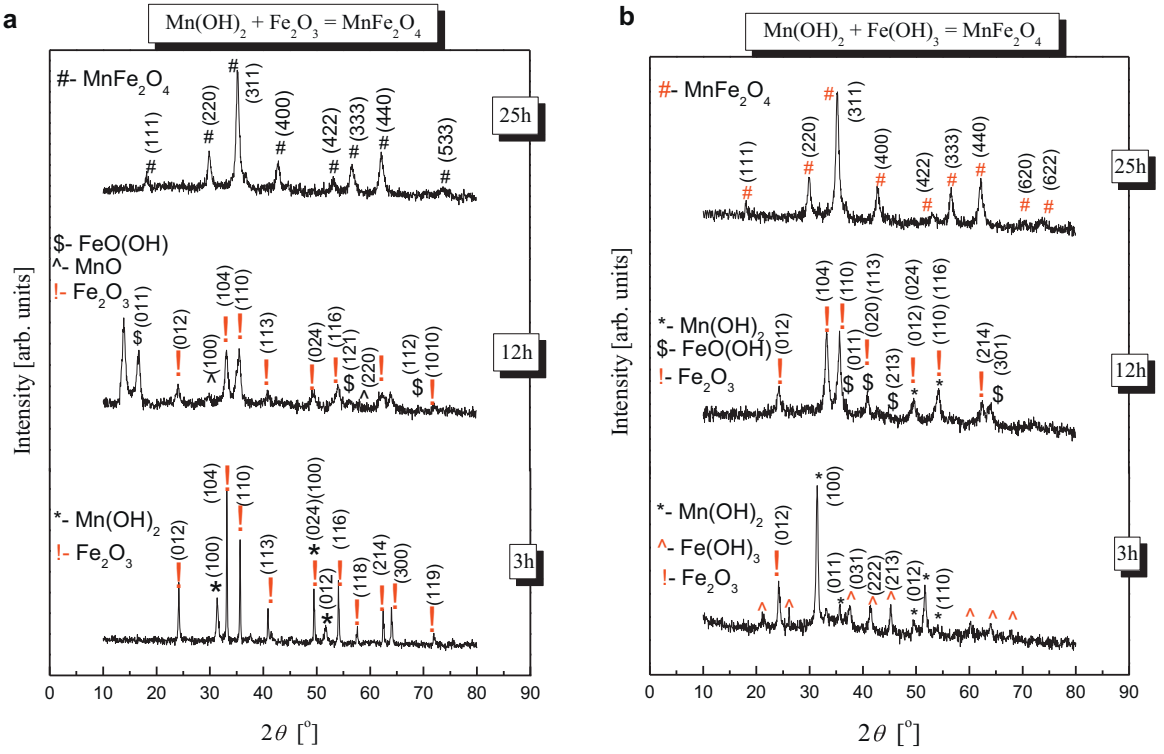

Fig. 1. X-ray diffraction pattern of the mixture of (a) $Mn(OH)_2$ and α-Fe_2O_3 and (b) $Mn(OH)_2$ and $Fe(OH)_3$ powders after various milling time.

Further milling up to 12 h leads to full synthesis of new phase. The appearance of the new peak at $2\theta = 18.09^\circ$, 29.89°, 35.37°, 42.85°, 53.11°, 56.76°, 62.13° and 73.74°, clearly indicates the formation of the new phase of $MnFe_2O_4$ (JCPDS card 74-2403) (Fig. 1a). The peaks are well indexed to the crystal plane of spinel ferrite ($k\,h\,l$) (1 1 1), (2 2 0), (3 1 1), (4 0 0), (3 3 3), (4 4 0) and (5 3 3), respectively. This confirms that the mechanochemical synthesis of $MnFe_2O_4$ is feasible and complete for 25 h milling time. Compared to other synthesis routes to $MnFe_2O_4$, the soft mechanochemical process used here represents a high-yielding, low-temperature and low-cost procedure for synthesis of nanocrystalline $MnFe_2O_4$ [22,28,29].

XRD pattern of powders in case (b) mechanically milled for 3, 12 and 25 h were shown in Fig. 1b. Before any mechanochemical treatment only sharp peaks from the well crystallized starting materials were present in the XRD pattern, expect for $Fe(OH)_3$ sample, where X-ray analysis confirmed that it was amorphous, with small amount of crystalline phase. In case (b), the full spectra of $Mn(OH)_2$ (JCPDS card 73-1133) and $Fe(OH)_3$ (JCPDS card 38-0032) characteristic peaks were present. Therefore, after 3 h there were no too many peaks corresponding to the starting compound $Mn(OH)_2$. $Mn(OH)_2$ quickly decomposed through $Mn(OH)_2 \rightarrow MnO + H_2O$. MnO peaks (JCPDS card 75-1090) could not be seen indicating that amorphization of manganese oxide had occurred. In the full spectrum of $Mn(OH)_2$, $Fe(OH)_3$ and α-Fe_2O_3 characteristic peaks were present, indicating that opposed to case (a), no decomposition of either of the starting components had occurred. After 3 h of milling time, in Fig. 1b, it can see the appearance of peaks characteristic for FeO(OH) (JCPDS card 89-6096). Most probably it was the consequence of the presence and separation of water from $Fe(OH)_3$ (via $Fe(OH)_3 \rightarrow FeO(OH) + H_2O$). At the same time XRD pattern ($2\theta = 40.89^\circ$), indicating that composition of iron(III)-hydroxide to hematite (Fig. 1b). Same as in the case (a), in the case (b) the new phase of $MnFe_2O_4$ is clearly identified by milling for 25 h. The pattern of $MnFe_2O_4$ could be indexed using cubic spinel cell space group in both cases synthesis.

In both cases, the conditions for soft milling existed since the synthesis took place in the presence of water (water vapour), which took part in the reactions as a damper of collisions between the balls and the material. Nevertheless, due to the small amount of water which separates from $Fe(OH)_3$ and $Mn(OH)_2$ during the synthesis of $MnFe_2O_4$, and periodic opening of the milling vessel to remove water vapour overpressure, formation of the new phase was accomplished.

Crystallite size of powders were calculated by means of Scherrer equation (S) [30] treated mechanochemically for 25 h were determined using XRDP data as:

$$S = \frac{0.9\lambda}{B\cos\theta_B}$$

where S is the crystallite grain size, λ is the wavelength of the X-ray source, θ_B is the Bragg angle of the considered XRDP peaks, and B represents the FWHM line broadening obtained as follows:

$$B^2 = B_m^2 - B_s^2$$

where B_m is the FWHM line broadening of the material and B_s represents the FWHM line broadening of the internal standard (α-Al_2O_3) [30]. The resulting value of the crystallite size, obtained from the (3 1 1) strongest reflections, is 40 and 50 nm respectively for cases denoted by (a) and (b) after 25 h milling times.

Raman spectroscopy is a non-destructive material characterization technique and is sensitive to structural disorder. It provides an important tool to probe the structural properties of mechanosynthesized materials. $MnFe_2O_4$ has a cubic structure that belongs to the space group O_h7 ($Fd3m$). Although the supercell contains 56 atoms ($Z = 8$), the primitive cell only consists of 14 atoms ($Z = 2$). As a result, the factor group analysis predicts the following modes in $MnFe_2O_4$:

$$\Gamma = A_{1g}(\mathrm{R}) + E_g(\mathrm{R}) + F_{1g} + 3F_{2g}(\mathrm{R}) + 2A_{2u} + 2E_u + 4F_{1u}(\mathrm{IR}) + 2F_{2u}$$

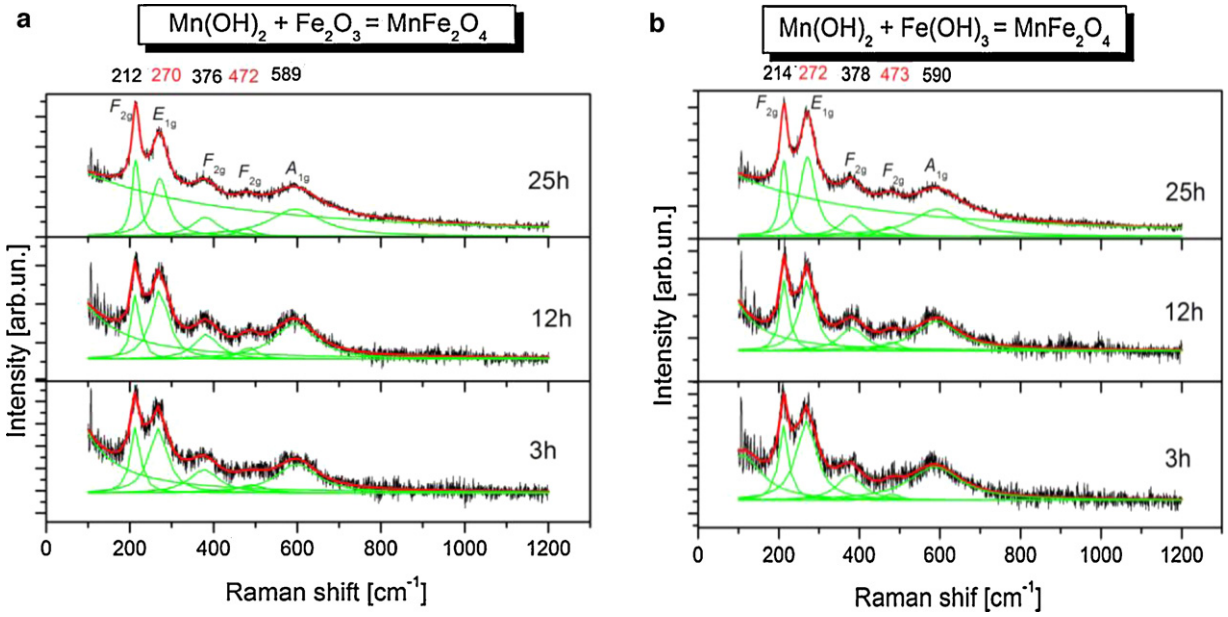

Fig. 2. Raman spectra at room temperature of the mixture of: (a) $Mn(OH)_2$ and α-Fe_2O_3 and (b) $Mn(OH)_2$ and $Fe(OH)_3$ powders after various milling time.

The F_{1g}, A_{2u}, E_u and F_{2u} modes are silent. There are five first-order Raman active modes ($A_{1g} + E_g + 3F_{2g}$), and all these modes were observed at ambient conditions, as shown in Fig. 2. The A_{1g} mode is due to symmetric stretching of oxygen atoms along Fe–O bonds, E_g and F_{2g} (3) are due to symmetric and asymmetric bending of oxygen with respect to Fe, respectively and F_{2g} (2) is due to asymmetric stretching of Fe and O, F_{2g} (1) is due to translational movement of the whole FeO_4 (Fe at tetrahedral site along with four oxygen atoms). Here, the notation A is for one dimensional representation, E for two and F for three dimensional representations, g and u denote symmetry and anti symmetry with respect to the centre of inversion. Raman active modes of $MnFe_2O_4$ measured in spectral region between 100 and 1200 cm^{-1} at ambient conditions. In the cubic ferrites, the modes at above 600 cm^{-1} mostly correspond to the motion of oxygen in tetrahedral AO_4 groups [31], so the mode at 589 cm^{-1} for case (a) and the mode at 590 cm^{-1} for case (b) of synthesis can be reasonably considered as A_g symmetry. The other low frequency modes represent the characteristics of the octahedral sites (BO_6). On other hand, it can be concluded that the high oxygen bends are observed in the range 600–500 cm^{-1}, corresponds to intrinsic stretching vibrations of the metal at the tetrahedral site, $M_{tetra} \leftrightarrow O$, whereas the lowest band, usually observed in the range 480–365 cm^{-1}, is assigned to octahedral–metal stretching, $M_{octa} \leftrightarrow O$. The mode, observed at around 589 cm^{-1} for $MnFe_2O_4$ can be assigned to tetrahedral Mn^{2+} stretching, and band observed at 472 cm^{-1} involves the Fe^{3+} vibration at the octahedral site. The five first-order Raman modes at about 212, 269, 376, 472 and 589 cm^{-1} for both cases synthesis exhibit the broad characteristics (Fig. 3a and b). The obtained tree modes at about 212, 376 and 472 cm^{-1} for case (a) of synthesis, and 214, 378 and 473 cm^{-1} for case (b) of synthesis belong to the symmetry type F_{2g}. Also, it can see that the modes 270 and 272 cm^{-1} belong to same symmetry E_g for case (a) and (b), respectively. By increasing the milling time, the grain size is being reduced. When reducing the grain size, quantum effects are coming to the forefront. Raman spectra are often analyzed with the help of a Lorentzian curve. Only 5 Raman bands are clearly observed. More deep Raman and IR study will be the subject of future investigations.

The position of the Raman modes, obtained by deconvolution, is presented in Fig. 3. The position change with increasing of milling times is expressed for all 5 active Raman modes. Analysis error is about 5%.

Fig. 4 shows the SEM micrographs for the sample obtained from the mixture of (a) $Mn(OH)_2$ and Fe_2O_3 and (b) $Mn(OH)_2$ and $Fe(OH)_3$ powders by the soft mechanochemical synthesis after 12 and 25 h milling time, respectively. The powder dissolved in kerosene was de-agglomerated in ultrasonic bath before analysis. The images reveal that beside observed agglomerates, which could not be destroyed in above mentioned process, the material is rather amorphized due to fact that it was not possible to distinguish separate particles. The tendency to be agglomerated increase with milling time. The individual particle size was very difficult to determine due to indistinct image at higher magnification. The size of the powder particles of the starting powders mixture varied. As result of mechanochemical reaction, the powders become much finer and uniform in shape. While the starting powder mixture consisted predominantly of individual particles, the sample of mechanosynthesized manganese

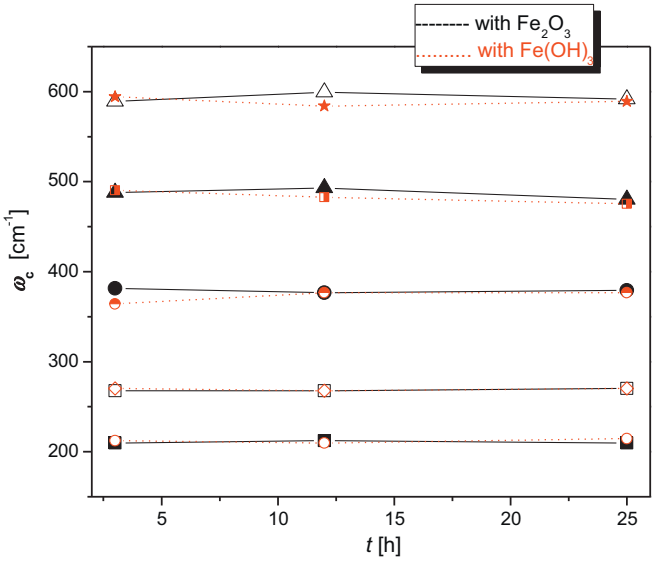

Fig. 3. Position of Raman modes.

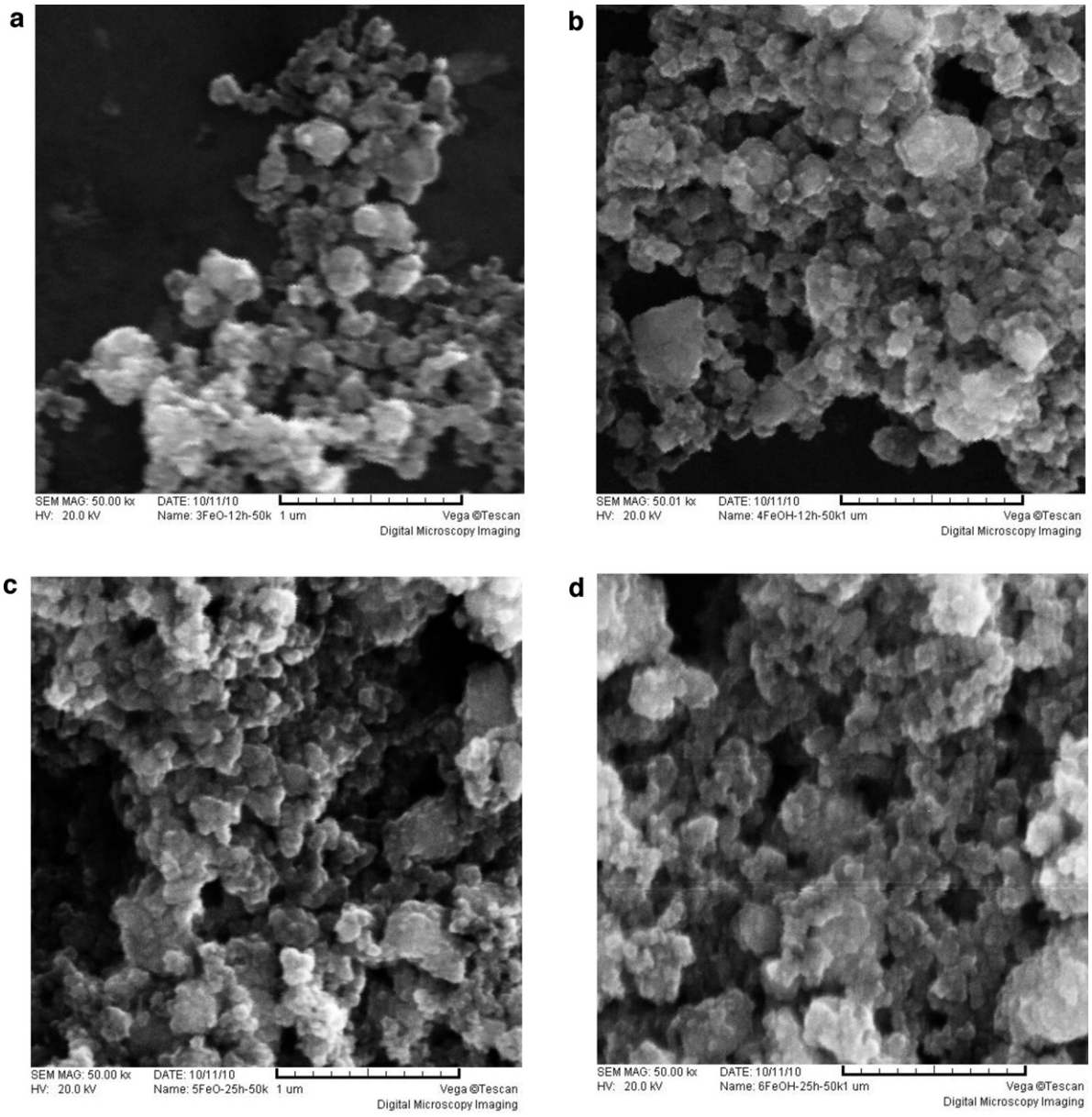

Fig. 4. SEM images of nanoscale mechanosynthesized of $MnFe_2O_4$ after 12 h and 25 h of milling of the mixture of: (a) $Mn(OH)_2$ and α-Fe_2O_3 and (b) $Mn(OH)_2$ and $Fe(OH)_3$ powders, respectively.

ferrite consists of aggregates of fine particles. The shape of the majority of the crystallites appeared to be spherical. As shown in Fig. 4 nanoscale crystallites tended to agglomerate because of dipolar field of each crystallite. Agglomerated crystallites formed grains with sizes mostly up to 50 nm for mixture of powders after 12 h milling time. The synthesized $MnFe_2O_4$ ferrite had a nanocrystalline structure with a crystallite size of about 20 and 30 nm for cases the sample obtained from the mixture of (a) $Mn(OH)_2$ and Fe_2O_3 and (b) $Mn(OH)_2$ and $Fe(OH)_3$ after 25 milling time.

In the investigated samples the product $MnFe_2O_4$ appears in the form of nanocrystalline particles after longer milling times. In the samples milled for 6 h starting materials and intermediate reaction products dominate the EDP patterns. The sample with starting composition $Fe(OH)_3$ and $Mn(OH)_2$ shows more product than the sample with the starting composition of α-Fe_2O_3 and $Mn(OH)_2$ after milling for 6 h each. Spinel-type reflections are barely visible in the EDP pattern in the sample where starting materials were hydroxides of both metals. Their relative intensity suggests than not more than 20% of $MnFe_2O_4$ is present in this sample. After, the samples are milled for 25 h most of the starting materials are reacted to the $MnFe_2O_4$ phase. The appearance of crystallites in both samples is similar, as well as the apparent degree of conversion. The average size of $MnFe_2O_4$ nanocrystals is between 10 and 50 nm and is fairly homogeneous for the sample with the α-Fe_2O_3 + $Mn(OH)_2$ starting composition, whereas that of the sample with the $Fe(OH)_3$ and $Mn(OH)_2$ starting composition ranges between 5 and 50 nm with some crystallites exceeding 100 nm (Fig. 5). The crystallites are rounded and tend to agglomerate into larger clusters with diameters of several hundred of nanometers. Measured *d*-values of $MnFe_2O_4$ are listed in Table 1. The images present in Fig. 6 reveal that the specimens consist of nanocrystalline particles and amorphous region with crystallite size about 50 nm that is in a good agreement with the crystallite size estimated from the XRD study. The composition of the product was confirmed by EDS measurements of several individual particles, as well as larger crystal

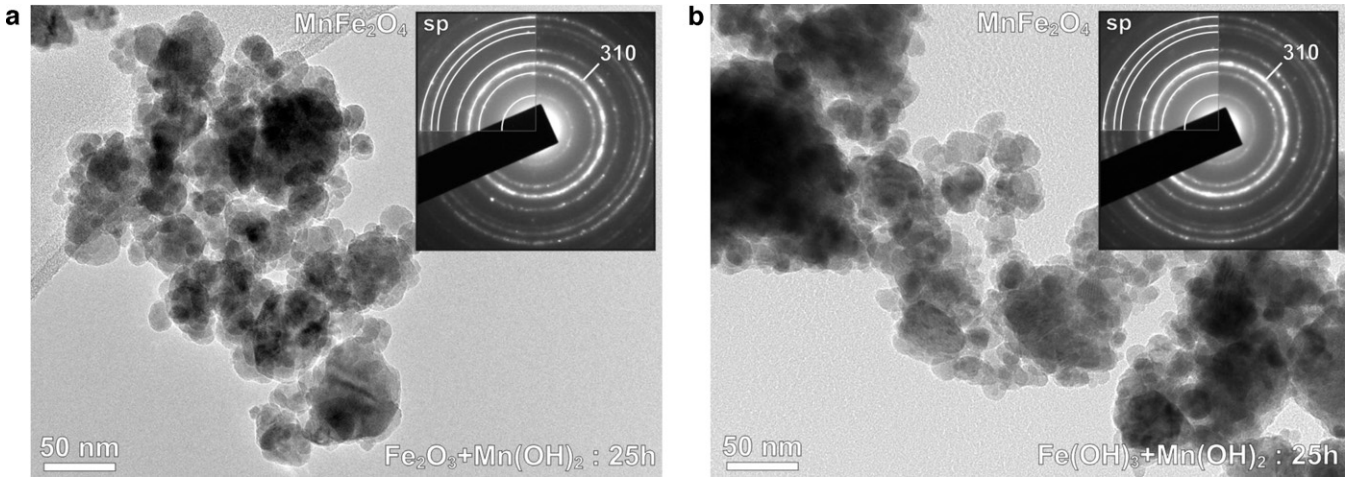

Fig. 5. TEM image with corresponding EDP of (a) $Mn(OH)_2$ and α-Fe_2O_3 and (b) $Mn(OH)_2$ and $Fe(OH)_3$ after milling for 25 h. Spinel-type reflections dominate the diffraction pattern (*inset*).

Table 1
Measured *d*-values (nm) for $MnFe_2O_4$ from EDP pattern (from Fig. 6).

	D_1	D_2	D_3	D_4	D_5	D_6	D_7
Measured (nm)	0.489	0.301	0.259	0.215	0.175	0.165	0.152
JCPDF #74-2403	0.49138	0.30090	0.25661	0.21277	0.17373	0.16379	0.15045
Crystallogr. plane	{111}	{220}	{311}	{400}	{422}	{333}	{440}

clusters. The analyses show a constant Mn:Fe atomic ratio of 1:2, which corresponds to the $MnFe_2O_4$ phase (Fig. 6).

The magnetic measurements were performed at room temperature and results for all samples were shown in Fig. 7 and Table 2. As could be seen, the magnetization showed almost the same dependence on milling time for both case of syntheses. At the start magnetization values were low, because, the reactions of formatting of $MnFe_2O_4$ phase did not start before the degradation and size reduction of mixtures of precursors. For powders α-Fe_2O_3 the magnetization remarkably increased after 1 h of milling and reached the maximum at 3 h [32]. The magnetization during first few hours could be attributed to α-Fe_2O_3 while considerably higher values of our samples corresponded to be contribution of ferrite phase. For milling times up to 3 h magnetization increased slowly,

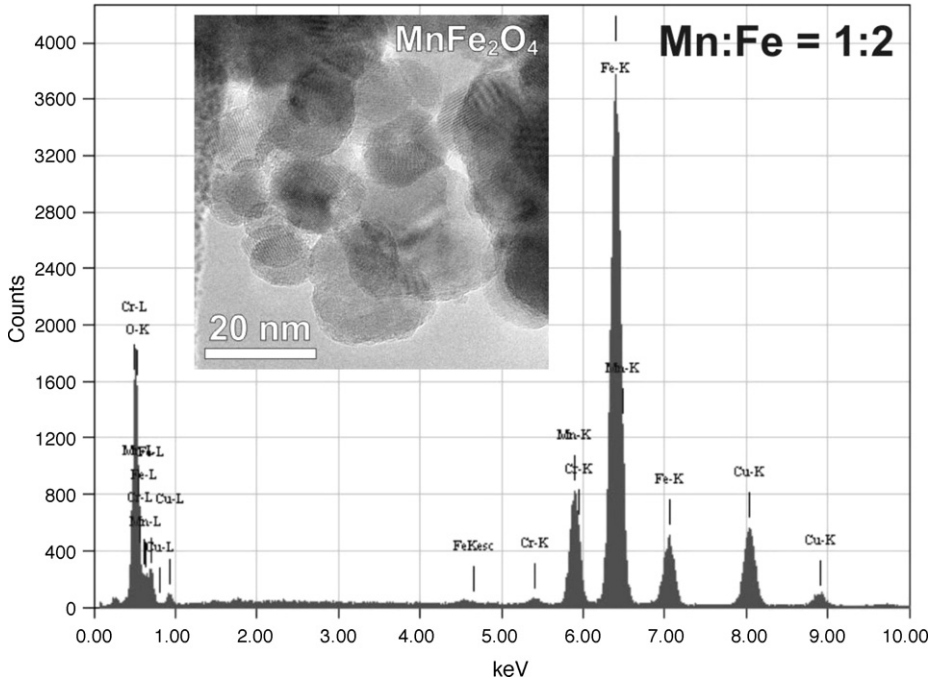

Fig. 6. EDS spectrum of $Mn(OH)_2$ and α-Fe_2O_3 after milling for 25 h shows the presence of single $MnFe_2O_4$ phase. The inset shows a HRTEM image of rounded $MnFe_2O_4$ nanoparticles with well resolved lattice fringes, characteristic for the spinel structure. Cu peak stems from the Cu-grid of the TEM specimen, whereas the minor peak of Cr could not be explained.

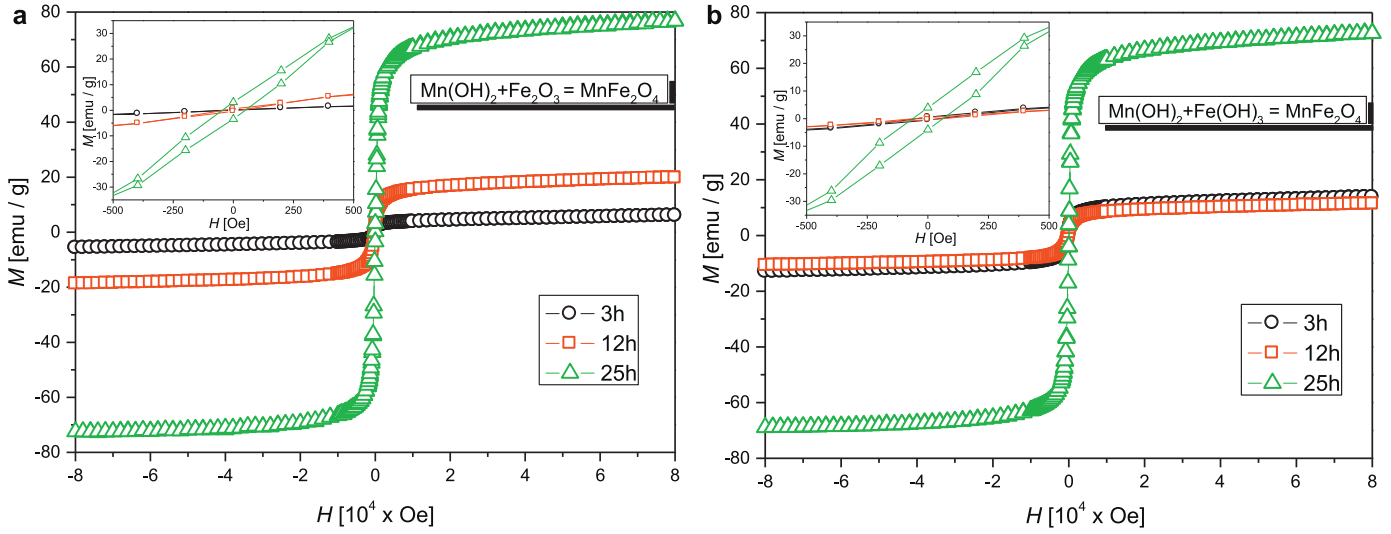

Fig. 7. The magnetic hysteresis curves of the mixture of: (a) $Mn(OH)_2$ and α-Fe_2O_3 and (b) $Mn(OH)_2$ and $Fe(OH)_3$ powders after various milling time. The *inset* shows low magnetization behavior.

Table 2
Magnetization measurements of the samples for the different milling time (3, 12 and 25 h) of the mixture powders.

Milling time (h)	*M* (emu/g)	
	$Mn(OH)_2 + \alpha$-Fe_2O_3	$Mn(OH)_2 + Fe(OH)_3$
3	4.8	12.3
12	15.8	10.2
25	70.4	71.1

indicating some structural changes. For the sample milled for 12 h, the increase in the magnetization was a result of the partial conversion of starting materials to the $MnFe_2O_4$ spinel phase. The slower change from 3 to 12 h could be attributed to the influence of water vapor evolution. After 12 h the surplus of water vapor was eliminated from the system by periodically opening the milling vessel. Results of magnetic measurement after 25 h of milling showed that the sample obtained from the mixture of $Mn(OH)_2$ and Fe_2O_3 powders had higher percent of formed $MnFe_2O_4$ phase then the sample obtained from the mixture of $Mn(OH)_2$ and $Fe(OH)_3$ powders. On other hand, room temperature hysteresis curves for the sample obtained from the mixture of (a) $Mn(OH)_2$ and Fe_2O_3 and (b) $Mn(OH)_2$ and $Fe(OH)_3$ powders after various milling time are shown in Fig. 7. These curves show the absence of coercive field, indicating the superparmagnetic behavior of the material. Also, they are typical of soft ferrites, however, complete magnetic saturation is not achieved even at 70 kOe. The spontaneous magnetizations, M_s are very similar (70.4 and 71.1 emu/g), that is smaller than the value for bulk $MnFe_2O_4$, 80 emu/g [33], and increases with milling time and decreases with crystallite size. This is consistent with the assertion that can be found in the work Aslibeiki et al. [20]. An increase in magnetization with the annealing temperature or milling time can be attributed mainly to the enhancement of crystallite size and crystallinity of samples. The increasing of magnetization by increasing milling time could be ascribed to the lower surface canting and surface disorder of the larger magnetic nanoparticles [20,34]. Also the low values of the saturation magnetization of these nanoparticles (compared to the bulk value, about 80 emu/g in manganese ferrite) [33,35] may be due to the presence of a magnetic dead layer or disordered layer on the surface of nanoparticles. These magnetically disordered states at grain surface are due to the high degree of contamination, breaking of Fe–O–Fe paths, deviation of stoichiometric composition, termination of crystal structure and dislocation. The change in magnetization is very intensive between 12 h and 25 h, showing that the mechanochemical reaction mainly takes place in this time interval (Fig. 7, Table 2). The measurement of the coercivity warrants the determination of the magnetization response with better accuracy and resolution particularly at small applied fields. Hence, a separate set of hysteresis curves was showed for each sample with an applied field of −500 to 500 Oe at room temperature (*the inset M–H* curves in Fig. 7a and b). While the *M–H* curve shows no hysteresis and no saturation for the mixture of (a) $Mn(OH)_2$ and Fe_2O_3 and (b) $Mn(OH)_2$ and $Fe(OH)_3$ powders obtained by the soft mechanochemical synthesis for 3 h and 12 h milling time, respectively. The absence of saturation, remanent magnetization and coercivity in *M–H* curves indicates the superparamagnetic nature of the materials. By the increasing the milling time to 25 h, the coercivity of samples are increasing and reaches to a coercivity of $H_c \approx 500$ Oe. It shows a small hysteretic behavior of samples obtained for 25 h at room temperature. The maximum magnetization for $MnFe_2O_4$ ferrites obtained for 25 h of milling time from the mixture of (a) $Mn(OH)_2$ and Fe_2O_3 and (b) $Mn(OH)_2$ and $Fe(OH)_3$ powders is quite interesting for such small nanoparticles, and is due to the crystallinity of the obtained samples. It is also well known that milling parameters can significantly influence the microstructural evolution including nanocrystallinity or amorphization during mechanical alloying [25]. The synthesis conditions are demonstrated to have a clear influence on their saturation magnetization (Fig. 7, *insets*). The hysteresis curve at low applied fields shows the values of the coercive field, $H_c \approx 500$ Oe and the remnant magnetization, $M_r \approx 32$ emu/g for sample obtained for 25 h of milling time from the mixture of (a) $Mn(OH)_2$ and Fe_2O_3 and (b) $Mn(OH)_2$ and $Fe(OH)_3$ powders. The saturation magnetization measured on the $MnFe_2O_4$ spinel ferrite nanopowder by a soft mechanochemical synthesis is higher than that for spinel ferrites produced by polymeric precursor [8]. The way we performed the extrapolation of results obtained by magnetic measurements at room temperature is the same as that which can be found in works by many authors [36–38].

Fig. 8 shows two Mössbauer spectra for samples obtained at room temperature from the mixture of: (a) $Mn(OH)_2$ and α-Fe_2O_3 and (b) $Mn(OH)_2$ and $Fe(OH)_3$ powders after 25 h milling time. The

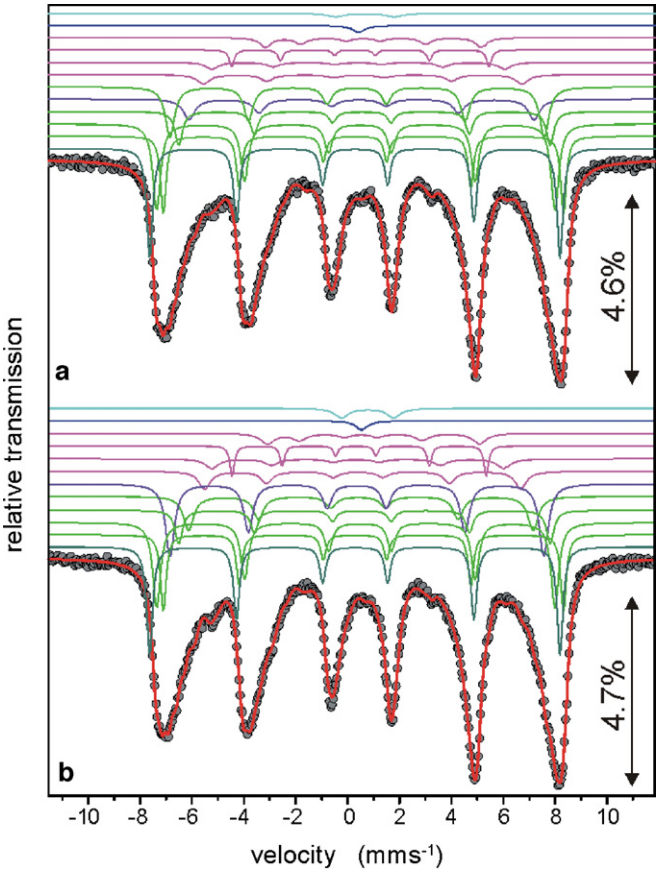

Fig. 8. Mössbauer spectra at room temperature of the mixture of: (a) $Mn(OH)_2$ and α-Fe_2O_3 and (b) $Mn(OH)_2$ and $Fe(OH)_3$ powders after 25 h milling time.

Mössbauer spectra for both samples consist of the twelve subspectra. They are divided in the three groups, depending of the particles size. A large nanoparticle requires five subspectra to describe cation distribution at the mixed spinel $(Mn_xFe_{1-x})^T(Mn_{1-x}Fe_{1+x})^MO_4$. The first sextet is assigned to ferric ion at tetrahedral site (*T*) with the cubic point symmetry group *Td*. It is confirmed with zero quadrupole splitting. Cations at this site feel the strongest antiferromagnetic hyperfine interaction as result of the superexchange interaction via oxygen ions. The ferric ions positioned at octahedral coordination site (*M*) show four sextets due to different local environment. The ferric cations at (*M*) site are very sense to the distribution of cations at (*T*) site [39]. Therefore, the belonged sextets have broadened line widths. The octahedral site has the trigonal point symmetry *D3d* group, and one expects certain electric field gradient EFG. The strength of hyperfine induction depends of distance between the magnetic ions and angle of Fe–O–Fe bonds. Also, the strength decreases as the volume of particles decreases. The superparamagnetic relaxation effect occurs at very small nanoparticles and we cannot observe a sextet any more, as consequence. We found that are presented the one doublet and the singlet, originated in octahedral and tetrahedral coordination, respectively. The cation site preference is affected when the size of particles are small, too. We found out in the first sample obtained of the mixture of $Mn(OH)_2$ and α-Fe_2O_3 powders after 25 h milling time amount of Mn^{2+} at tetrahedral site decrease from 76% to 51%, as size of particles decreased (Table 3). Also, tetrahedral preference of Mn^{2+} decreases from 80% to 54% as function of particle size at the second sample obtained from the mixture of $Mn(OH)_2$ and $Fe(OH)_3$ powders after 25 h milling time (Table 3).

Table 3
Mössbauer parameters for the mixture of powders of $Mn(OH)_2$ and α-Fe_2O_3 (*sample 1*) and $Mn(OH)_2$ and $Fe(OH)_3$ (*sample 2*) after milling of 25 h: δ – isomer shift with reference to α – Fe, Δ – quadruple splitting (2ε-shift), B – hyperfine induction, Γ – line width (FWHM) and A – relative area fraction of component. For site occupancies by cations Fe^{3+} are used signs: *T* for tetrahedral and *M* for octahedral site coordination.

Sample	δ (mm s^{-1})	Δ (mm s^{-1})	B (T)	Γ (mm s^{-1})	A (%)	Site
2						
	0.286(5)	−0.014(8)	49.04(5)	0.27(2)	15.2	T
	0.447(6)	0.33(2)	47.82(6)	0.26(3)	9(2)	M
	0.395(6)	−0.16(2)	47.59(7)	0.36(3)	21(5)	M
	0.60(2)	0.10(2)	44.4(1)	0.34(6)	7(2)	M
	0.48(1)	0.10(2)	41.2(1)	0.54(8)	11(3)	M
	0.36(1)	0.01(1)	44.7(1)	0.43(4)	17(3)	T
	0.52(2)	0.14(5)	38.1(2)	0.6(1)	6(2)	M
	0.41(3)	0.01(5)	35.0(2)	0.6(1)	5(1)	M
	0.39(2)	0.21(4)	30.8(1)	0.22(7)	1.5(4)	M
	0.80(2)	0.40(5)	25.8(2)	0.53(6)	4.9(7)	M
	0.43(3)			0.6(2)	1.2(3)	T
	0.66(6)	2.3(1)		0.8(2)	1.2(3)	M
1						
	0.275(5)	−0.040(8)	48.97(6)	0.27(2)	11.7	T
	0.422(6)	0.30(2)	47.82(5)	0.29(2)	11(2)	M
	0.376(6)	−0.18(2)	47.68(7)	0.35(3)	18(5)	M
	0.60(1)	0.10(2)	44.40(8)	0.32(4)	7(2)	M
	0.460(7)	0.10(1)	41.20(9)	0.48(4)	11(2)	M
	0.354(8)	0.008(8)	44.69(6)	0.42(3)	18(3)	T
	0.49(1)	0.18(3)	37.8(1)	0.54(6)	7(1)	M
	0.36(2)	0.06(4)	34.9(2)	0.64(9)	6(1)	M
	0.38(1)	0.13(2)	30.36(9)	0.21(4)	1.8(4)	M
	0.75(2)	0.50(3)	25.3(2)	0.65(5)	6.1(9)	M
	0.54(3)			0.6(1)	1.0(2)	T
	0.77(2)	2.01(6)		0.64(8)	1.4(2)	M

4. Conclusions

In this paper, we show that it is possible to obtain $MnFe_2O_4$ ferrite by soft mechanochemical synthesis starting from the mixture of (a) $Mn(OH)_2$ and α-Fe_2O_3 and (b) $Mn(OH)_2$ and $Fe(OH)_3$ powders. Ball milling was a suitable technique for the preparation of nanocrystalline $MnFe_2O_4$ ferrite. It has been shown that mechanochemical treatment of mixtures with starting materials lead to the amorphization of the starting powders and to their partial reaction, producing after 3 h of milling a mixture $Mn(OH)_2$ and Fe_2O_3, after 12 h of milling a mixture Fe_2O_3, MnO and FeO(OH), and finally after 25 h $MnFe_2O_4$, for case (a). On the other hand, observing case (b), after 3 h of milling starting powders can be observed in the presence of $Mn(OH)_2$, $Fe(OH)_3$ and Fe_2O_3, after 12 h of milling a mixture Fe_2O_3, $Mn(OH)_2$ and FeO(OH), and finally after 25 h $MnFe_2O_4$. It could be concluded that mechanochemical treatment leads to the successful formation of ultrafine powders of $MnFe_2O_4$ ferrite. On the basis of Raman research is observed five first-order Raman active modes. The intensity of the Raman modes in the formation of ferrite phase in both cases of synthesis are very close of values, but there are differences which indicates that milling leads to phase changes in the development of ferrite use soft mechanochemical method. More deep Raman study will be the subject of future investigations. The magnetic measurements after 25 h of milling show magnetization value of 70.4 emu/g and 71.1 emu/g. The Mössbauer spectra show the one doublet and the singlet, originated in octahedral and tetrahedral coordination, respectively. The cation site preference is affected when the size of particles are small, too. We found out in the both cases synthesis amount of Mn^{2+} at tetrahedral site decrease as size of particles decreased. This simple, low cost route should be applicable for the synthesis of other functional nanoparticles materials.

Acknowledgements

This research was financially supported by the Serbian Ministry of Science and Technological Development through Project Nos. III45003 and P141027.

References

[1] M.J.N. Isfahani, M. Myndyk, D. Menzel, A. Feldhoff, J. Amighian, V. Šepelák, J. Magn. Magn. Mater. 321 (2009) 152–156.
[2] X. Hou, J. Feng, X. Xu, M. Zhang, J. Alloys Compd. 491 (2010) 258–263.
[3] R.C. Kambale, P.A. Shaikh, S.S. Kamble, Y.D. Koleka, J. Alloys Compd. 478 (2009) 599–603.
[4] T.F. Marinca, I. Chicinas, O. Isnard, V. Pop, F. Popa, J. Alloys Compd. 509 (2011) 7931–7936.
[5] A.M.M. Farea, S. Kumara, K.M. Batoo, A.Y.C.G. Lee, Alimuddin, J. Alloys Compd. 469 (2009) 451–457.
[6] Z. Wang, D. Schiferl, Y. Zhao, H.St. C. O'Neill, J. Phys. Chem. Solids 64 (2003) 2517–2523.
[7] V. Sepelak, I. Bergmann, A. Feldhoff, P. Heitjans, F. Krumeich, D. Menzel, F.J. Litterst, S.J. Campbell, K.D. Becker, J. Phys. Chem. C 111 (2007) 5026–5033.
[8] M. Popa, P. Bruna, D. Crespo, J.M.C. Moreno, J. Am. Ceram. Soc. 91 (2008) 2488–2494.
[9] J.P. Chen, C.M. Sorensen, K.J. Klabunde, G.C. Hadijpanayis, E. Devlin, A. Kostikas, Phys. Rev. B 54 (1996) 9288–9296.
[10] D.M. Schleich, Y. Zhang, Mater. Res. Bull. 30 (1995) 447–452.
[11] L. Zhen, K. He, C.Y. Xu, W.Z. Shao, J. Magn. Magn. Mater. 320 (2008) 2672–2675.
[12] Y. Köseoğlu, M. Bay, M. Tan, A. Baykal, H. Sözeri, R. Topkaya, N. Akdoğan, J. Nanopart. Res., doi:10.1007/s11051-010-9982-6.
[13] R.V. Mangalaraja, S. Anathakmar, P. Monohar, F.D. Gnanam, M. Awana, J. Mater. Sci. Eng. A 367 (2004) 301–305.
[14] N. Kasapoğlu, A. Baykal, Y. Köseoğlu, M.S. Toprak, Scr. Mater. 57 (2007) 441–444.
[15] M.A. Ahmed, E.H. El-Khawas, F.A. Radwan, J. Mater. Sci. 36 (2001) 5031–5035.
[16] M.H. Mahmoud, H.H. Hamdeh, J.C. Ho, M.J. O'Shea, J.C. Walker, J. Magn. Magn. Mater. 220 (2000) 139–146.
[17] M. Muroi, R. Street, P.G. McCormick, J. Amighian, Phys. Rev. B 63 (2001) 184414.
[18] J. Ding, P.G. McCormick, R. Street, J. Magn. Magn. Mater. 171 (1997) 309–314.
[19] F. Padella, C. Alvani, A. La Barbera, G. Ennas, R. Liberatore, F. Varsano, Mater. Chem. Phys. 90 (2005) 172–177.
[20] B. Aslibeiki, P. Kameli, H. Salamati, M. Eshraghi, T. Tahmasebi, J. Magn. Magn. Mater. 322 (2010) 2929–2934.
[21] P. Osmokrovic, C. Jovalekic, D. Manojlovic, M.B. Pavlovic, J. Optoel. Adv. Mater. 8 (2006) 312–314.
[22] E. Avvakumov, M. Senna, N. Kosova, Soft Mechanochemical Synthesis: A Basis for New Chemical Technologies, Kluwer Academic Publishers, Boston, 2001.
[23] V. Šepelák, D. Baabe, F.J. Litterst, K.D. Becker, J. Appl. Phys. 88 (2000) 5884–5893.
[24] M.J. Nasr Isfahani, M. Myndyk, V. Šepelák, J. Amighian, J. Alloys Compd. 470 (2009) 434–437.
[25] V. Šepelák, K.D. Becker, J. Mater. Synth. Process. 8 (2000) 155–166.
[26] R.A. Brand, Nucl. Instrum. Meth. Res. B 28 (1987) 398.
[27] Joint Committee on Powder Diffraction Standards (JCPDS) Powder Diffraction File (PDF), International Centre for Diffraction Data, Newton Square, PA, 2003.
[28] S.P. Gubin, Yu.A. Koksharov, G.B. Khomutov, G.Yu. Yurkov, Russ. Chem. Rev. 74 (6) (2005) 489–520.
[29] I. Chicinas, J. Optoel. Adv. Mater. 8 (2006) 439–448.
[30] B.E. Warren, Scherrer and Warren equations, in: X-ray Diffraction, Addison Wesley, Reading, MA, 1969.
[31] Z.W. Wang, P. Lazor, S.K. Saxena, G. Artioli, J. Solid State Chem. 165 (2002) 165–170.
[32] M. Zdujic, C. Jovalekic, Lj. Karanovic, M. Mitric, D. Poleti, D. Skala, Mater. Sci. Eng. A 245 (1998) 109–117.
[33] R.S. Tebble, D.J. Craik, Magnetic Materials, Wiley-Interscience, London, 1969.
[34] Z. Gu, X. Xiang, G. Fan, F. Li, J. Phys. Chem. C 112 (2008) 18459–18466.
[35] V.A.M. Brabers, in: K.H.J. Buschow (Ed.), Handbook of Magnetic Materials, vol. 8, Elsevier Science, New York, 1995, pp. 197–212.
[36] Y. Köseoğlu, A. Baykal, F. Gözüak, H. Kavas, Polyhedron 28 (2009) 2887–2892.
[37] M. Sertkol, Y. Köseoğlu, A. Baykal, H. Kavas, A. Bozkurt, M.S. Toprak, J. Alloys Compd. 486 (2009) 325–329.
[38] H. Kavas, A. Baykal, M.S. Toprak, Y. Köseoğlu, M. Sertkol, B. Aktas, J. Alloys Compd. 479 (2009) 49–55.
[39] M. Siddique, N.M. Butt, Physica B 405 (2010) 4211–4215.